Tyrosine kinase inhibitor prodrug-loaded liposomes for controlled release at tumor microenvironment

Stefano Salmaso [a,1], Francesca Mastrotto [a,1], Marco Roverso [b], Valentina Gandin [a], Sara De Martin [a], Daniela Gabbia [a], Michele De Franco [a], Christian Vaccarin [a], Marco Verona [a], Adriana Chilin [a], Paolo Caliceti [a], Sara Bogialli [b], Giovanni Marzaro [a,*]

[a] Department of Pharmaceutical and Pharmacological Sciences, University of Padova, via Marzolo 5, 35131, Italy
[b] Department of Chemistry, University of Padova, via Marzolo 1, 35131, Italy

A B S T R A C T

Tyrosine kinase inhibitors (TKIs) represent one of the most advanced class of therapeutics for cancer treatment. Most of them are also cytochrome P450 (CYP) inhibitors and/or substrates thereof. Accordingly, their efficacy and/or toxicity can be affected by CYP-mediated metabolism and by metabolism-derived drug-drug interactions. In order to enhance the therapeutic performance of these drugs, we developed a prodrug (**Pro962**) of our TKI **TK962** specifically designed for liposome loading and pH-controlled release in the tumor. A cholesterol moiety was linked to **TK962** through pH-sensitive hydrazone bond for anchoring to the liposome phospholipid bilayer to prevent leakage of the prodrug from the nanocarrier. Bioactivity studies performed on isolated target kinases showed that the prodrug maintains only partial activity against them and the release of **TK962** is required. Biopharmaceutical studies carried out with prodrug loaded liposomes showed that the prodrug was firmly associated with the vesicles and the drug release was prevented under blood-mimicking conditions. Conversely, conventional liposome loaded with **TK962** readily released the drug. Flow cytometric studies showed that liposomes efficiently provided for intracellular prodrug delivery. The use of the hydrazone linker yielded a pH-controlled drug release, which resulted in about 50% drug release at pH 4 and 5 in 2 h. Prodrug, prodrug loaded liposomes and active lead compound have been tested against cancer cell lines in either 2D or 3D models. The liposome formulation showed higher cytotoxicity than the unformulated lead **TK962** in both 2D and 3D models. The stability of prodrug, prodrug loaded liposomes and active lead compound in human serum and against human, mouse, and rat microsomes was also assessed, demonstrating that liposome formulations impair the metabolic reactions and protect the loaded compounds from catabolism. The results suggest that the liposomal formulation of pH releasable TKI prodrugs is a promising strategy to improve the metabolic stability, intracellular cancer cell delivery and release, and in turn the efficacy of this class of anticancer drugs.

1. Introduction

Kinase inhibitors, especially tyrosine kinase inhibitors (TKIs), have been largely investigated as anticancer agents [1–3]. Their mechanism of action relies on impairment of the catalytic activity of kinases, thus inhibiting the proliferative signaling cascade [3]. TKIs, while having high structural diversity, share some common features including high lipophilicity and few chemical homologies (*i.e.*, a nitrogen-containing heterocycle, a hydrophobic moiety, and a solvent-exposed moiety) that endow them with ATP mimicking structure [3,4]. The hydrophobic moiety is crucial to modulate the selectivity of TKIs toward the tyrosine kinases [4]. On the other hand, the portion of the TKIs solvent-exposed after binding with the kinase can be functionalized with a variety of moieties without impairing their pharmacodynamic activity [4,5]. In this perspective, we recently reported that by virtue of their diarylurea portion as hydrophobic moiety, *N*-phenyl-*N*′-[4-(pyrimidin-4-ylamino) phenyl]urea derivatives can selectively inhibit a few members of the class III receptor tyrosine kinase (RTKs; namely FLT3, cKIT, and PDGFRβ) family [5]. Class III RTKs are known oncogenes and their role in cancer onset and progression has been reported [6]. Besides, we have

---

shown that the further functionalization of the urea moiety with fluorine-containing functions results in enhanced inhibition of RET (Rearranged during Transfection) kinase [7]. This family of derivatives is of remarkable interest since both class III RTKs and RET are involved in the cancer onset [6,8–10], and these compounds showed *in vitro* anticancer activities comparable to those of the FDA approved drugs sunitinib and vandetanib [5,7], and promising *in vivo* activity (low systemic toxicity along with anticancer properties) [5].

TKIs have been found to be substrates of cytochrome P450 (CYP) isoforms, which are responsible for their liver catabolism [11], while at high doses they behave as CYP inhibitors [12]. Consequently, co-administration with other drugs undergoing the same enzymatic processing can lead to drug-drug interactions due to CYP inhibition. The metabolites of TKIs are more hydrophilic than the parent compounds and generally still active [11]. However, whether they still maintain the kinase selectivity profile of the parent drug has not been clearly demonstrated. We recently reported that derivatives with high hydrophilicity may possess low kinase selectivity [5], which may yield side effects due to off-target interactions. Thus, strategies that minimize TKIs metabolism may be beneficial for their safety.

Several TKIs have been found to possess low access to the cytosolic space. For such a reason, several compounds that showed strong binding to isolated tyrosine kinases, for example PD153035, dramatically failed when tested in cells [13]. One of the most exploited chemical strategy to enhance cell internalization is the functionalization of the solvent-exposed region of TKIs with protonatable functions (*e.g.*, piperazine moieties as in the case of gefitinib, imatinib, ponatinib [14]), that in a few cases can enhance cell entry by exploiting organic cation transporters [15]. Additionally, protonation can increase the water solubility of the derivative and thus its bioavailability also upon oral administration.

Colloidal carriers, such as nanoparticles and vesicles, can be properly exploited to yield intracellular delivery of TKI derivatives. Liposomes, in particular, have been largely exploited by virtue of their safety and versatility to deliver both hydrophilic and lipophilic drugs [16,17]. The liposome-mediated drug delivery ensures protection of loaded drugs from catabolism by preventing the interaction with metabolizing enzymes during blood circulation [18]. However, loading efficiency may represent a critical issue in liposome development. For such a reason, different strategies to enhance the drug loading have been developed, including remote loading for hydrophilic charged drugs, or lipophilic anchors to exploit the large bilayer surface [19–22]. Furthermore, while liposomes can passively dispose in the tumor site by enhanced permeation and retention (EPR) mechanism, the control of drug release requires additional strategies to modulate the diffusive release across liposome membrane. A successful example of liposomal formulation is Doxil, where high doxorubicin loading and slow release have been obtained by inducing drug nano-crystallization in the aqueous core of liposomes [23,24]. On the other side, TKIs loading into liposomes and controlled release are limited by their high diffusivity through the vesicle lipid bilayer, while nano-crystallization in the aqueous core of liposomes cannot be generally exploited for this class of molecules.

In order to develop the prototype of a formulation for controlled TKI delivery, we explored the generation of a TKI prodrug to anchor the drug to the lipidic bilayer and control the release within the acid cancer cell compartments (*i.e.*, endosomes and lysosomes). Accordingly, the TKI moiety has been derivatized with a cholesteryl moiety through a pH-sensitive hydrazone bond. We investigated the prodrug and released drug activity against isolated kinases and in cancer cell monolayer and 3D-cell model. Liposome formulations of the TKI prodrug were developed and biopharmaceutically characterized. To the best of our knowledge, this is the first study where a TKI was loaded in liposomes as prodrug according to a strategy that was aimed at both enhancing the loading and association to the carrier and controlling its release.

2. Materials and methods

2.1. Materials

All solvents and starting materials were purchased from commercial suppliers (Sigma Aldrich and Carlo Erba) and used without further purifications. The thin layer chromatography (TLC) was performed on pre-coated plates of silica gel 60 with fluorescent indicator UV254 (0.2 mm, Merck); column chromatography was performed with silica gel 60 (0.063–0.100 mm, Merck). Flash chromatography was performed on a Biotage Isolera instrument (Uppsala, Sweden). The microwave-assisted synthetic procedures were conducted on a CEM Discover (Italy) mono-mode reactor with the temperature monitored by a built-in infrared sensor and the automatic control of the power; all the reactions were performed in closed devices with pressure control. The ^{1}H NMR spectra were recorded at room temperature on a Bruker 400-AMX spectrometer (Billerica, MA, USA); chemical shifts are reported in ppm and are referred to residual solvent signals. Liposome extrusion was performed using an Avanti mini extruder (Avanti Polar Lipids Inc. Alabaster, AL, USA).

Human pancreatic (BxPC3 and PSN-1) carcinoma cell lines were obtained from the American Type Culture Collection (ATCC, Rockville, MD). Human cervical (A431) carcinoma cells were kindly provided by Prof. F. Zunino (Division of Experimental Oncology B, Istituto Nazionale dei Tumori, Milan, Italy). Cell lines were maintained in the logarithmic phase at 37 °C in a 5% carbon dioxide atmosphere using Roswell Park Memorial Institute (RPMI)-1640 cell culture medium containing 10% fetal bovine serum (Euroclone, Milan, Italy), antibiotics (50 units/mL penicillin and 50 μg/mL streptomycin), and 2 mM L-glutamine (Euroclone, Milan, Italy). Pooled human liver microsomes (HLMs) were purchased from BD Gentest (New Jersey, USA). Electrospray ionization mass spectra were collected on a Xevo G2-XS QTof (Waters) by direct injection of the sample. The UHPLC-HRMS/MS system was equipped with an Ultimate 3000 UHPLC chromatograph coupled with a Q Exactive™ hybrid quadrupole-Orbitrap™ mass spectrometer (Thermo Fisher Scientific, Waltham, Massachusetts, USA). HPLC experiments were conducted on a Shimadzu SPD10-AVP instrument equipped with the UV-VIS detector set at 263 nm. The column used for HPLC analysis was a Phenomenex Gemini C18 5 μm, 250 × 4.6 mm. For mass spectrometric analysis all reagents and solvents used were HPLC or LC-MS grade. MilliQ water was obtained with a Millipore system (18.2 MΩ*cm). Acetonitrile and formic acid (99%) were purchased from VWR Chemicals (Radnor, USA) and Carlo Erba (Milano, Italy), respectively.

2.2. Synthesis, solubility and pH-stability of compounds

See Supplementary data for detailed description of compound synthesis and characterization. Structures of compounds are reported in Fig. 1A (**TK962**) and 1F (**Pro962** and **Ctrl962**) in Results and Discussion (3.1 Rationale).

2.2.1. Solubility of compounds in aqueous media

TK962, **Pro962** or **Ctrl962** were dissolved in DMSO at a final concentration of 10 mM. Ten microliters of the DMSO solutions were added to 990 μL of 10 mM phosphate buffer, 0.15 M NaCl (PBS), pH 7.4, or the same buffer supplemented with increasing amounts of DMSO (up to 10%, final volume) or PBS, pH 7.4, supplemented with 10% FBS. The mixtures were stirred at 37 °C overnight, centrifuged at 6000 rpm for 5 min. In the case of samples containing FBS, 100 μL solutions were added of 300 μL acetonitrile and centrifuged at 12,000 rpm for 10 min. All supernatants were analysed by RP-HPLC to assess the **TK962**, **Pro962** or **Ctrl962** concentration by using a Phenomenex Gemini C18 5 μm, 250 × 4.6 mm and eluted with tetrahydrofuran:acetonitrile 70:30 (eluent A) and methanol (eluent B) with a linear gradient from 20% to 80% of A in 20 min. The UV detector was set at 263 nm. All the calibration curves are reported in Figs. S1-S3.
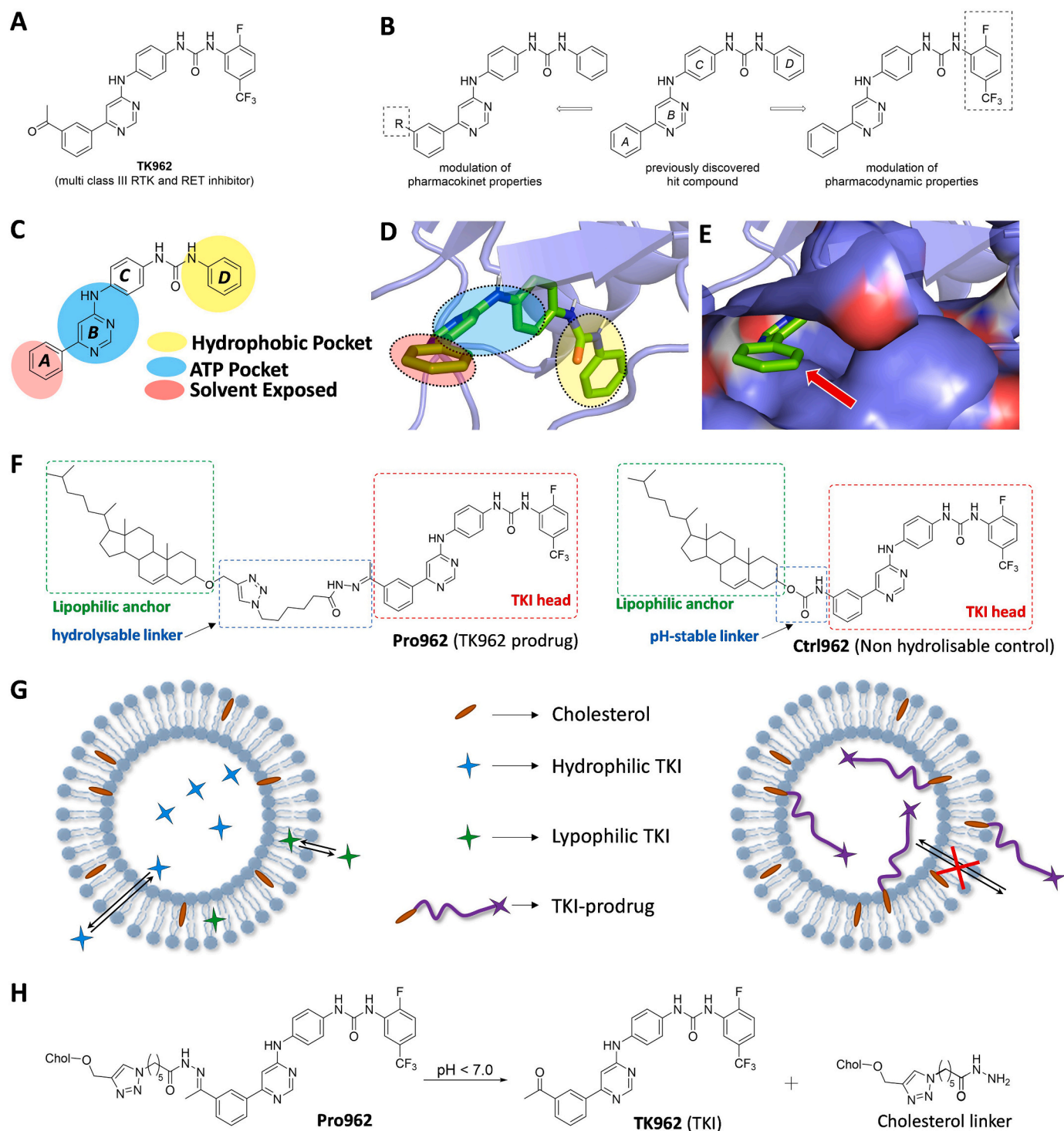
Fig. 1. Rationale of the work.

2.2.2. pH-dependent hydrolysis

Pro962 or **Ctrl962** were dissolved in PBS at different pHs of 4.0, 5.0, 6.5 or 7.4, supplemented with 10% DMSO (final compound concentration: 15 μM) and stirred at 37 °C for 72 h. At scheduled time points (Table S2) the solutions were analysed by RP-HPLC as reported above. The amounts of both starting and hydrolysed compounds were assessed.

2.3. Liposome formulation and characterization

2.3.1. Liposome formulation

Liposomes were prepared according to the thin-film hydration process reported in the literature [25]. Briefly, 238 μL of 6.7 mg/mL egg phosphatidylcholine (EPC) in CHCl$_3$ were mixed with fixed volumes of 5.0 mg/mL cholesteryl conjugated prodrugs in CHCl$_3$ and 6.7 mg/mL cholesterol in CHCl$_3$ in a 10 mL round bottom flask to yield 2 mg total lipid. The amount of cholesterol was adjusted on the basis of the cholesteryl conjugated prodrug to yield a final 2:1 EPC/cholesterol (free

cholesterol + TKI-conjugated cholesterol) molar ratio. The organic solvent was removed under reduced pressure at 37 °C using a rotary evaporator. Then the lipid film was hydrated with 1 mL of 10 mM phosphate buffer, pH 7.4. The lipid dispersion underwent 10 freeze-and-thaw cycles. Dispersions were extruded for 11 cycles through a polycarbonate membrane with a nominal pore diameter of 200 nm, which allowed for both liposome size reduction and homogenisation and elimination of undissolved drug. Due to the very low solubility of **Pro962** and **Ctrl962** in aqueous media (< 1 μg/mL), the unloaded prodrug precipitated and remained entrapped on the membrane.

Conventional liposomes were prepared according to the above reported method by adding 238 μL of 6.7 mg/mL egg phosphatidylcholine (EPC) in $CHCl_3$ and 60.7 μL of 6.7 mg/mL cholesterol in $CHCl_3$ to 7.8 μL of 10 mM **TK962** in $CHCl_3$ in a 10 mL round bottom flask to yield 2 mg total lipid.

Fluorescently labelled liposomes were prepared by including rhodamine B-1,2-dihexadecanoyl-sn-glycero-3-phosphoethanolamine (rhodamine-DHPE) in $CHCl_3$ lipid/prodrug or lipid/**TK962** solution at a 0.3% mol ratio with respect to lipids.

The encapsulation efficiency and capacity of prodrugs in liposomes were assessed after liposome formulation by quantifying the amount of compound loaded in the liposomes through RP-HPLC analysis as follow: lyophilized liposomes were dissolved in 1 mL of water and 20 μL of sample was diluted to 500 μL with acetonitrile. 10 μL of the organic solution were injected in a Phenomenex Gemini C18 5 μm, 250 × 4.6 mm and eluted with tetrahydrofuran:acetonitrile 70:30 (eluent A) and methanol (eluent B). The eluent mixture changed linearly from 20% of A to 80% of A in 20 min. The signals were detected at 263 nm.

The Loading Efficiency (LE) and Loading Capacity (LC) were assessed, according to Eqs. (1) and (2):

$$LE = \frac{\text{fraction of loaded drug } (\mu g)}{\text{fed drug } (\mu g)} \cdot 100 \qquad (1)$$

$$LC = \frac{\text{loaded drug } (\mu g)}{\text{total lipids } (\mu g)} \bullet 100 \qquad (2)$$

2.3.2. Size and zeta potential analysis, and stability

The size and polydispersity index (PDI) of liposomal formulations or Pro962 in PBS, pH 7.4, were measured by photo correlation spectroscopy (PCS) using a Zetasizer NanoZS (Malvern Instrument LTD, Malvern, UK). The liposome dispersions were diluted before analysis with 10 mM phosphate buffer, pH 7.4, to a concentration of 0.5 mg/mL. Zeta potential was measured using a Zetasizer NanoZS upon dilution of liposome dispersions in mQ water to 0.5 mg/mL. Pro962 samples were prepared by diluting 10 μL of 10 mM prodrug in DMSO with 990 μL PBS, pH 7.4. The samples were centrifuged at 6000 rpm for 5 min and the supernatant was analysed.

The liposome colloidal stability was performed by incubating 2 mg/mL drug loaded liposomes in 10 mM phosphate buffer, pH 7.4, at 4 °C and 40 °C for 7 days. At scheduled times, the samples were diluted to 0.5 mg/mL with 10 mM phosphate buffer, pH 7.4, and analysed by PCS.

2.4. In vitro studies

2.4.1. Cell viability assays

The growth inhibitory effect toward tumor cells was evaluated by MTT assay [26]. Briefly, $3–8 \times 10^3$ cells/well, depending on the growth rates of the cell line, were seeded in 96-well microplates in cell culture medium (100 μL). After 24 h, the medium was removed and replaced with a fresh medium containing the compound to be studied (either **Pro962**, **Ctrl962**, **TK962** or Sunitinib dissolved in pure DMSO – 10 mM stock solution, or **Lipo2-Pro962** or **Lipo4-Ctrl962** reconstituted in PBS) at 0–16 μM concentration. Each treatment was performed in triplicate. After 72 h, each well was added of 10 μL of a 5 mg/mL 3-[4,5-dimethylthiazol-2-yl]-2,5-diphenyl tetrazolium bromide (MTT) saline

solution, and incubated for 5 h at 37 °C under 5% CO_2 atmosphere. Afterwards, the medium was removed and 100 μL of a sodium dodecyl sulfate (SDS) solution in 0.01 M HCl was added. After overnight incubation at room temperature, cell viability was assessed by measuring the absorbance at 570 nm using a Bio-Rad 680 microplate reader (Hercules, CA, USA). Mean absorbance for each derivative equivalent concentration was expressed as a percentage of the control untreated cell absorbance and plotted *vs* drug concentration. IC_{50} values, the drug concentrations that reduce the mean absorbance at 570 nm to 50% of those of untreated control wells, were calculated by the four parameters logistic (4-PL) model. Evaluation was based on means from at least four independent experiments.

2.4.2. Spheroid cultures and APH assay

Spheroid cultures were obtained by seeding $1.5–2.5 \times 10^3$ human pancreatic (BxPC3 and PSN-1) or human cervical (A431) cancer cells/well in a round bottom non-tissue culture treated 96-well plate (Greiner Bio-one, Kremsmünster, Austria) in phenol red free RPMI-1640 medium containing 10% FBS and supplemented with 20% methyl cellulose stock solution. After 72 h, the medium was removed and replaced with fresh medium containing the compound to be studied (either **Pro962**, **Ctrl962**, **Lipo2-Pro962**, **Lipo4-Ctrl962**, **TK962** or Sunitinib) at the appropriate concentration. A modified acid phosphatase (APH) assay, which is based on the quantification of the cytosolic acid phosphatase activity, was used to determine the cell viability in spheroids [27]. After 72 h, the medium was removed and each well was treated with 100 μL of the assay buffer (0.1 M sodium acetate, 0.1% Triton-X-100, supplemented with ImmunoPure *p*-nitrophenyl phosphate; Sigma Chemical Co., Darmstadt, Germany) and, after 3 h of incubation, 10 μL of 1 M NaOH solution was added. The inhibition of the cell growth induced by the tested compounds or formulations was detected by measuring the absorbance of each well at 405 nm, using a Bio-Rad 680 microplate reader. Each treatment was carried out in triplicate. The mean absorbance for each drug dose was expressed as a percentage of the control untreated well absorbance (T/C) and plotted *vs* the derivative equivalent concentration. IC_{50} values (the drug concentrations that reduce the mean absorbance values at 405 nm to 50% of those in the untreated control wells) were calculated by the four-parameter logistic (4-PL) model. The evaluation was based on the means of at least four independent experiments.

2.4.3. Cell association of rhodamine-loaded Lipo2-Pro962 (Rho-Lipo2-Pro962) or rhodamine Lipo4-Ctrl962 (Rho-Lipo4-Ctrl962)

A431 and PSN-1 cells were seeded in RPMI-1640 added of 10% FBS at a density of 1.5×10^5 cells/well in a 24-well plate and grown overnight at 37 °C, 5% CO_2 under a controlled atmosphere. The medium was then discarded, and cells underwent different treatments:

- A431 cell line: the medium was replaced with 400 μL/well of 84 μg/mL fluorescently labelled and prodrug **Pro692**-loaded liposomes in RPMI medium containing 10% FBS or opti-MEM® added of 1% FBS.
- A431 and PSN-1 cell lines: the medium was replaced with 400 μL/well of 84 μg/mL fluorescently labelled prodrug **Pro692** or **Ctrl962**-loaded liposomes in RPMI medium containing 10% FBS.

After 24 h of incubation the cells were rinsed three times with 1 mL of 0.15 M NaCl, 20 mM phosphate, pH 7.4 (phosphate buffered saline, PBS), detached by treatment with 200 μL of a 0.0625% *w/v* trypsin solution in PBS and fixed with 1% PFA in PBS until FACS analysis. Cells were analysed with BDCANTOII and data were elaborated with the FLOWJO software v10. At least 2×10^4 events were acquired per sample.

2.4.4. Stability in human plasma and with liver microsomes

Pro962 and **TK962** were dissolved in human plasma supplemented with 1% NaN_3 to reach a final compound concentration of 20 μM.

Similarly, **Lipo2-Pro962** was dispersed in the same medium to yield a **Pro962** equivalent concentration of 20 μM. All samples were incubated at 37 °C and 100 μL volumes were collected at 30 min, 1, 2, 4, 8, 16, 24 and 48 h. The samples were diluted with 300 μL of acetonitrile. After centrifugation for 10 min at 12,000 g, supernatants were collected and analysed by RP-HPLC as reported above to assess the hydrolytic stability of the compounds.

Mouse and rat liver microsomes were prepared from hepatic tissues as already described [28]. Metabolic stability was assessed by incubating **Pro962**, **TK962** or **Lipo2-Pro962** with mouse, rat and human microsomes [29]. Briefly, 10 μM solutions of **Pro962** and **TK962** or **Pro962** equivalent **Lipo2-Pro962** were incubated at 37 °C for 10, 20, or 30 min in a reaction mixture (400 μL), containing 200 μg of microsomal proteins and 10 mM NADPH in 0.1 M phosphate buffer, pH 7.4. At the end of incubation, the reaction was stopped by adding 200 μL acetonitrile. After centrifugation for 10 min at 12,000 g, supernatants were collected and analysed by RP-HPLC as reported above to assess the metabolic stability of tested derivatives and catabolite formation. The effect of human microsomes on compounds and liposome formulation was further investigated by means of high resolution-mass spectrometric (HRMS) analysis, suggesting the structures of the formed metabolites.

Structures of the compounds treated with human microsomes were also analysed without further sample purification by UHPLC-HRMS/MS in order to identify the structures of formed metabolites. The UHPLC-HRMS/MS system was equipped with an Ultimate 3000 UHPLC chromatograph coupled with a Q Exactive™ hybrid quadrupole-Orbitrap™ mass spectrometer (Thermo Fisher Scientific, Waltham, Massachusetts, USA). A Kinetex 2.6 μm EVO C18, 100 A, 100 × 2.1 mm (Phenomenex, Bologna, Italy) column thermostated at 40 °C was used as stationary phase, and water+0.1% formic acid was used as eluent A, while eluent B was THF:acetonitrile 70:30 + 0.1% formic acid. The chromatographic gradient was as follow: 0–2 min 5% B, 2–17 min, 5%–100% B; 17–22 min, 100% B; 22–23 min, 100%–5% B; 23–30 min, 5% B. The flow rate was set to 0.25 mL/min. MS data were acquired in electrospray (ESI) positive ionization mode; resolution was set at 35,000 in MS and 17,500 in MS/MS; AGC target $3 \cdot 10^6$ in MS and $2 \cdot 10^5$ in MS/MS; max injection time: 100 ms; scan range: 250–2000 *m/z*; isolation window: 2.0 *m/z*; collision gas: nitrogen, normalized collision energy (NCE): 35. Capillary voltage was 4.0 kV, capillary temperature 320 °C, and auxiliary gas was nitrogen at 40 psi. Calibration was performed with a standard solution purchased by Thermo Fisher Scientific (Pierce® ESI positive Ion Calibration Solution). Possible metabolic by-products of the selected compounds were simulated by the Biotransformation Mass Defects software (Agilent Technologies, Palo Alto, CA, USA) and resulting signals were searched for in the acquired chromatograms with a mass accuracy of 5 ppm. Structures of identified compounds were confirmed by MS/MS experiments.

2.4.5. In vitro release of compounds from Lipo4-Ctrl962, Lipo2-Pro962 and conventional liposome

The formulations **Lipo2-Pro962**, **Lipo4-Ctrl962** or **Lipo1-TK962** at 2 mg/mL lipid concentration were dialyzed at 37 °C for 48 h using a 300-kDa cut-off Float-A-Lyzer® G2 system using 1 L of PBS at different pHs (pH 7.4 for **Lipo1-TK962**; pH 7.4, 6.5, 5.0 and 4.0 for **Lipo2-Pro962** and **Lipo4-Ctrl962**) supplemented with 10% FBS as receiving medium. Five hundred microliter samples were collected at 30 min, 1, 2, 4, 8, 16, 24 and 48 h and diluted with 500 μL of acetonitrile. After centrifugation for 10 min at 12,000 g, 500 μL of supernatants were collected and dried under vacuum. The solid residue was resuspended in 20 μL of pure DMSO and analysed by HPLC as reported above to determine the amount of **Ctrl962** (in the case of **Lipo4-Ctrl962**), **Pro962** and **TK962** (in the case of **Lipo2-Pro962**) or **TK962** (in the case of **Lipo1-TK962**) released in solution.

2.5. Computational methodologies

All the computational methodologies were carried out on a 32 Core AMD Ryzen 93,905×, 3.5 GHz Linux Workstation (O.S. Ubuntu 20.04) equipped with GPU (Nvidia Quadro RTX 4000, 8 GB).

The structure of **Ctrl962** and **Pro962** were prepared with MarvinSketch 5.5.0.1 software (www.chemaxon.com/products). The *in vacuo* lowest energy conformation and the degree of protonation at pH 7.4 were determined with OpenBabel software [30] using the MMFF94s force field. Docking studies were conducted with AutoDock Vina software [31], while the MDs were conducted with the Gromacs software [32,33].

2.5.1. Docking studies

The tridimensional structure of human albumin was downloaded from the Protein Data Bank (PDB ID: 1ao6 [34]). The appropriate ". pdbqt" files for both albumin and **Pro962** were prepared according to literature [35] and a blind docking procedure was faced, *i.e.*, the docking box contained the whole protein [36]. The lowest energy binding pose was then analysed.

2.5.2. Molecular dynamics simulations

MDs were conducted under the Charmm36 force field. The suitable parameters for **Pro962** and **Ctrl962** were obtained through the CGenFF website [37,38]. A symmetric phospholipid bilayer of 8 × 8 lipids size per layer (128 lipids in total) was prepared using the CHARMM-GUI webserver [39]. To mimic the liposomes, the following bilayer composition was used: 40 x palmitoyloleoylphosphatidylcholine (POPC), 20 x palmitoyllaurylphosphatidylcholine (PLPC), 16 x stearoyloleoylphosphatidylcholine, 8 x stearoyllaurylphosphatidylcholine, 44 x cholesterol. 22.5 Å of water thickness layer were added on both top and bottom sides of the system, which was finally composed of 29,535 atoms. One cholesterol moiety was replaced by either **Pro962** or **Ctrl962** before steepest descent energy minimization was conducted. The systems were then equilibrated under first NVT and then NPT conditions for 100 and 200 ps respectively. Long range electrostatic interactions were modelled using the Particle Mesh Ewald algorithm. LINCS, Nosé-Hoover and Parrinello-Rahman algorithms were used in the simulations for restraints, and as thermostat and barostat respectively. MDs were conducted for 25 ns with 2 fs time steps. RMSD values, energies, compartment membrane density were calculated using the suitable functions implemented in Gromacs.

To investigate the aggregation at high concentration of **Ctl962**, 10 molecules of the compound were added to a previously equilibrated 15x15x15 Å box of solvent. The system was then equilibrated under first NVT and then three NPT cycle conditions for 100, 100, 200 and 300 ps respectively. NVT and the first NPT equilibrations were simulated constraining the positions of all the heavy atoms. In the second NPT equilibration, the solvent heavy atoms were unrestrained. In the third NPT equilibration, the whole system was unrestrained. Through these steps, the final density of the system was comparable to the density of the pure solvent and the system resulted stable. The MD was then conducted for 25 ns with 2 fs time steps.

2.6. Statistical analysis

Statistical analysis was performed with GraphPad Prism 7.0 (GraphPad Software, Inc., San Diego, CA) using one-way Anova and followed by the *post hoc* Turkey's multiple comparison test. All the data are presented as the mean ± standard error of the mean. Differences between groups were considered to be significant at a level of $p < 0.05$.

3. Results and discussion

3.1. Rationale

The rationale behind the present work is resumed in Fig. 1.

The rationale behind the design of the new multi class III RTKs and RET inhibitor bearing the *N*-phenyl-*N'*-[4-(pyrimidin-4-ylamino) phenyl]urea scaffold (**TK962**; Fig. 1A) is based on our previous findings, which showed that the functionalization of ring *A* of the hit compound (Fig. 1B, left) does not alter the selectivity profile of this class of compounds [5,7]. Interestingly, we showed that the ring *A* can be derivatized at *meta*-position to modify the pharmacokinetic behavior of the parent compound [5]. According to the simulated binding mode of the hit compound in cKIT kinase (Fig. 1C-D), the ring *A* occupies the solvent exposed region of the kinase ATP binding pocket. In particular, the *meta*-position of the ring points outwards from the kinase surface (Fig. 1E). Therefore, this position is suitable for substitution with small functional groups aimed at modulating the availability and, conceivably, the bioavailability of these drugs. Conversely, the functionalization at ring *D* (that occupies the hydrophobic pocket) modulates the selectivity of these compounds (Fig. 1B, right). Indeed, unsubstituted ring *D* results in the selective class III RTK inhibitors, whereas fluorine containing ring *D* results in a multi class III and RET kinase inhibitors [7].

According to these considerations, a prodrug of **TK962** was rationally designed (Fig. 1F, compound **Pro962**) with the aim to generate a multi class III RTK and RET inhibitor (by virtue of the fluorinated *N*-phenyl-*N'*-[4-(pyrimidin-4-ylamino)phenyl]urea portion) that could be loaded into liposomes by virtue of the cholesterol anchor to minimize unspecific and off-target drug release. Indeed, TKIs loaded into liposomes (either hydrophilic drug loaded in the inner core or lipophilic drugs in the lipid bilayer) could leak out and be released by diffusive process (Fig. 1G, left). Conversely, TKIs conjugated to cholesterol are expected to result in compounds more tightly anchored to the liposome lipid bilayer and the release before cell uptake can be prevented (Fig. 1G, right). Importantly, cholesterol is one of the components of the liposome bilayer and it exposes its hydroxyl group in position 3 toward the aqueous environment. Therefore, this hydroxyl group is available for chemical conjugation without interfering with the insertion of the polycyclic lipid in the lipid bilayer of liposomes [40]. Consequently, the prodrug **Pro962** can be released from liposomes only after cell uptake and the active compound **TK962** can be generated under the acidic conditions of lysosomes. Indeed, in compound **Pro962** cholesterol was conjugated to **TK962** through a pH sensitive linker (hydrazone), to yield

parent drug release under acidic conditions as reported in Fig. 1H. To investigate the effect of pH on drug release due to the linker cleavage, a cholesterol conjugate of the drug through a non-hydrolysable bond (carbamate) was synthesized (**Ctrl962**, non-hydrolysable control).

3.2. Kinase profiling of synthesized compounds

In a preliminary study, the affinity of **TK962** for a panel of tyrosine kinase targets has been assessed using the KinomeScan platform [41] in order to identify the best targets of this molecule (see Table S1 in Supplementary Data). Then, **TK962**, **Pro962** and **Ctrl962** were tested to assess their ability to bind the target kinases, which showed the highest affinity in the preliminary screening: FLT3, cKIT, PDGFRβ and RET (Table 1).

The results reported in Table 1 show that the Kd values obtained with **TK962** are similar to the ones previously published with the analogue without the carbonyl group in the ring *A* [5], indicating that this small chemical function, which is required for the cholesterol conjugation through the pH-sensitive bond, does not affect the molecule activity. **Pro962** possesses 13–20% of parent drug affinity, whereas **Ctrl962** does not show significant binding affinity for all the tested tyrosine kinases.
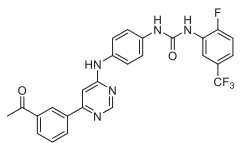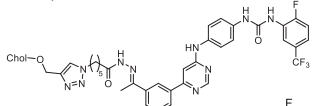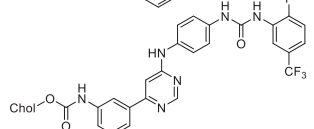
These results show that the anchoring moiety may have *per se* an influence on the drug affinity for the biological targets. Nevertheless, the method of conjugation may be detrimental for the target recognition and binding. In the case of **Pro962**, where cholesterol is attached to the parent drug through a flexible linker, the prodrug shows a decrease of affinity. On the contrary, the **Ctrl962**, which has been obtained by direct conjugation of cholesterol to the ring *A* of the TKI, is inactive.

Therefore, these results confirm the importance of linker engineering, as the direct binding of the cholesterol moiety (that is straightforward from a synthetic point of view) is detrimental for the affinity to the targets, whereas a more flexible linker allows an efficient, even if suboptimal, binding. However, it must be pointed out that the presence of a hydrolysable bond can allow the release of the parent drug, fully recovering the binding affinities.

3.3. Solubility and behavior of the compounds in aqueous media

The addition of the DMSO solution of **TK962** to PBS, pH 7.4, yielded a **TK962** maximum concentration of 65 ± 9 μM indicating that this drug is moderately soluble in aqueous buffer. On the contrary, the addition of DMSO stock solutions of **Pro962** and **Ctrl962** to PBS yielded less than 1 μM compound concentrations indicating that these molecules are poorly

Table 1
Affinity constants (Kd) of synthesized compounds. FLT3, cKIT and PDGFRβ belong to the class III RTK.

Compound	Structure	Kd (nM)[a]			
		FLT3	cKIT	PDGFRβ	RET
TK962		59	35	15	52
Pro962		290	230	90	380
Ctrl962		> 10,000	> 10,000	> 10,000	> 10,000

[a] Target kinase is indicated in the first line of each column.

soluble in physiologic buffer. Higher solubility was obtained by increasing the DMSO content in the buffer solution: about 20 µM **Pro962** and **Ctrl962** solutions were obtained with 10% of DMSO (Table S2). Dynamic light scattering (DLS) studies showed that upon addition of DMSO solutions to PBS, both **Pro962** and **Ctrl962** did not form micelles while large precipitating aggregates were clearly visible. **Pro962** and **Ctrl962** were even more soluble (30 ± 2 and 23 ± 4 µM, respectively) in PBS supplemented with 10% FBS. Molecular docking studies conducted with **Pro962** and human serum albumin (PDB ID: 1ao6) showed that the prodrug was able to strongly bind the protein, which is in agreement with the observed increased solubility of **Pro962** in the presence of FBS. Interestingly, the lipophilic moiety was predicted to occupy the binding site for testosterone [42], whereas the linker flexibility allowed the compound to well fit the protein surface (Fig. S4).

3.4. pH-dependent prodrug activation

The pH stability of **Pro962** and **Ctrl962** was investigated by incubating the compounds in PBS at different pHs mimicking lysosomes (pH 4.0), late endosomes (pH 5.0), endosomes (pH 6.5) and blood (pH 7.4). According to the solubility data reported above, 10% of DMSO was also added to ensure that compounds were completely solubilized in the buffers. **Ctrl962** was found to be chemically stable at all pHs over 72 h incubation (data not shown). On the contrary, the results reported in Fig. 2 and Table S3 show that **Pro962** has a pH dependent stability. **Pro962** was fairly stable at pH 7.4 while at acidic pH, the drug release was faster. In particular, at pHs mimicking the lysosome and late endosome conditions 50% of **TK962** was released from **Pro962** in 2 h, while at pH 6.5 more than 24 h were required to release 50% of drug.

3.5. Characterization and stability of liposomes

Seven liposome formulations were prepared according to the *thin film hydration* method [25] using different amounts of **Pro962** or **Ctrl962** and constant 2:1 EPC/cholesterol (free cholesterol + drug conjugated cholesterol) molar ratio: **lipo0** = 0% mol prodrug; **Lipo1-Ctrl962** and **Lipo1-Pro962** = 1% mol prodrug; **Lipo2-Ctrl962** and **Lipo2-Pro962** = 2.5% mol prodrug; **Lipo3-Ctrl962** and **Lipo3-Pro962** = 5% mol prodrug; **Lipo4-Ctrl962** and **Lipo4-Pro962** = 10% mol prodrug; **Lipo5-Ctrl962** and **Lipo5-Pro962** = 15% mol prodrug; **Lipo6-Ctrl962** and **Lipo6-Pro962** = 25% mol prodrug; **Lipo7-Ctrl962** and **Lipo7-Pro962** = 30% mol prodrug.

Liposomes with size in the range of 120–190 nm (Table S4 and S5) and 0.10–0.25 polydispersity (PDI) were obtained, regardless the liposome composition. The zeta potential was slightly negative (Table S4 and S5), which was in agreement with the zwitterionic feature of the EPC.
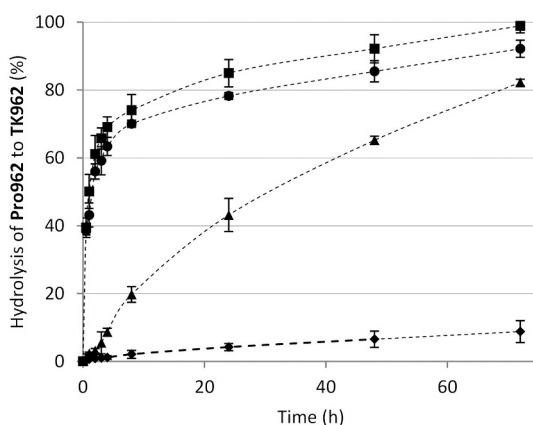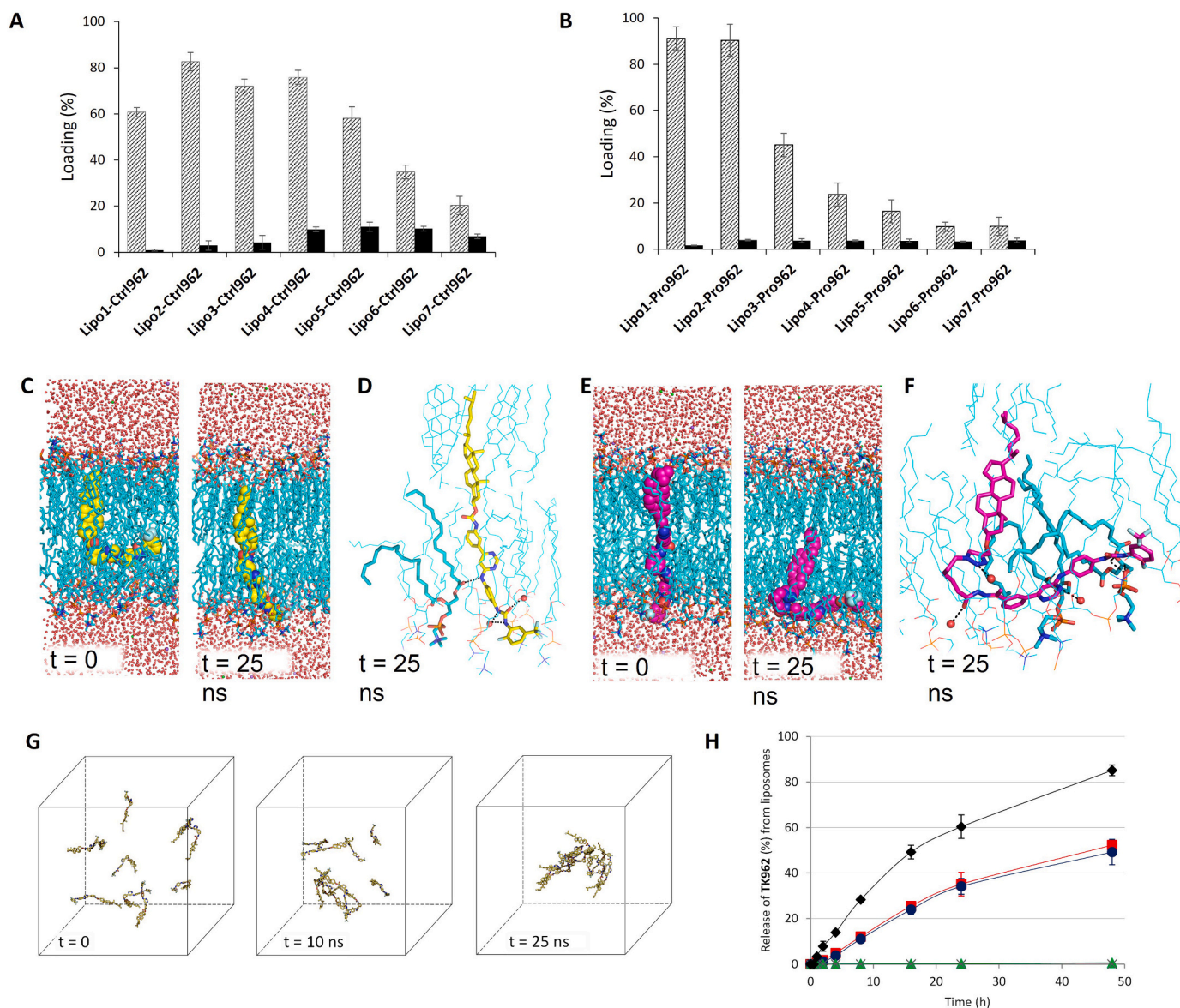
Fig. 3A,B shows the loading efficiency and capacity of **Pro962** and **Ctrl962** into liposomes. As expected, the loading efficiency of both derivatives was found to decrease with the increase of compound feeding in the lipid mixture used for the liposome preparation. However, over 60% loading efficiency was found up to 15% **Ctrl962** feeding (**Lipo5-Ctrl962**) and over 80% in the case of 1% and 2.5% **Pro962** feeding (**Lipo1-Pro962** and **Lipo2-Pro962**). The loading of **Ctrl962** remained almost constant between 10 and 25% feeding, and a maximum of 11% loading capacity (LC) of **Ctrl962** could be achieved in these conditions. At 30% **Ctrl962** feeding, a reduction in the LC to 6.9% was instead observed. In the case of **Pro962** the loading capacity readily reached a plateau, so that the amount of the loaded prodrug in the liposomes was fairly constant from 2.5% to 30% feeding with a maximum LC of 3.9%. The different loading behavior of the two prodrugs may be attributable to the different structure of the molecule conveyed by the cholesterol conjugation. Molecular dynamics simulations (MDs) showed that both **Ctrl962** or **Pro962** in a phospholipidic bilayer with composition similar to that used to prepare the liposome formulations reached the equilibrium within 10 ns and that these structures remained stable for further 15 ns simulations (Fig. S5A,B). As expected, the TKI head of the compounds established polar interactions with the phospholipid polar heads, while the lipophilic anchors were well inserted in the apolar core of the membrane (Fig. 3C,E). As expected, the interactions between the prodrugs and the bilayer were predominantly hydrophobic. Indeed, during the MDs, a strong negative short-range Lennard-Jones interaction potential (that estimates the Van der Waals interactions) was observed, while only in the case of **Pro962** we found that also short-range Coulomb interactions between the compound and the phospholipid heads contributed to stabilize the system (Fig. S5C,D). Interestingly, the TKI head of both the compounds did not protrude in the aqueous environment during the MDs, remaining entrapped in the inner space of the phospholipid heads where only few water molecules are present (Fig. 3D,F), as can be seen by the very low solvent-accessible surface area measured for both **Ctrl962** and **Pro962** (Fig. S5C,D). This is probably a consequence of the hydrophobic features of the anchoring cholesterol chains that tend to occupy the central part of the bilayer as shown by the compartment density analysis conducted on the MDs (Fig. S6). However, while the more rigid **Ctrl962** adopted a lower hindering "I" shape (Fig. 3C,D), **Pro962** resulted inserted in the bilayer with a more hindering "L" shape (Fig. 3E,F). These results were independent from the geometry initially used to place the compounds in the bilayer. Accordingly, we concluded that the liposome bilayer can accommodate a higher amount of the "I"-shaped **Ctrl962** than the "L"-shaped **Pro962**, explaining the different maximal loading capacity (11% and 3.9%, respectively). The slight decrease in LC measured at 30% **Ctrl962** feeding was also investigated through molecular dynamics. At this concentration, **Ctrl962** readily formed large aggregate in chloroform (*i. e.*, the solvent used for preparing the thin layer of lipids; Fig. 3G), while at lower concentration this phenomenon did not occur. Therefore, when using very high **Ctrl962** feeding percentage, a certain amount of the prodrug may be not available for the liposome loading.

Based on both loading efficiency and loading capacity values, **Lipo2-Pro962** and **Lipo4-Ctrl962** were selected for further biopharmaceutical characterization.

Both **Lipo2-Pro962** and **Lipo4-Ctrl962** were found to be colloidally stable over one week in buffer at pH 7.4, without significant alteration of size, PDI and *Z*-potential (Table S6 and S7).

The release of the loaded compounds (**Pro962** or **Ctrl962**) as well as of the parent drug **TK962** from the liposome formulations were assessed at different pH values. No release of **Ctrl962** was found under the experimental conditions. In the case of **Pro962** (Fig. 3H and Table S8), no release was found at pH 7.4 within 48 h, suggesting that the compounds were tightly associated to the liposome bilayer and confirming that under the pH condition mimicking the blood the hydrolysis of the **Pro962** does not occur. At acidic pH values, only **TK962** was released in solution from liposomes loaded with **Pro962**. The release of **TK962** was

Fig. 2. Hydrolysis profiles of **Pro962** to **TK962** incubated at different pHs (–■– pH = 4; –●– pH = 5; –▲– pH = 6.5; –◆– pH = 7.4).

Fig. 3. A, B: Loading efficiency (LE %, gray bars) and loading capacity (LC %, black bars) of liposomal formulation obtained by processing increasing prodrug/lipid molar ratio (A: **Pro962**; B: **Ctrl962**); C: Placement of **Ctrl962** in the phospholipidic bilayer at the beginning (t = 0) and at the end (t = 25 ns) of MDs; D: detail of the polar interactions between **Ctrl962** and the phospholipidic head and water molecules (red spheres) at the end of the MDs; E: Placement of **Pro962** in the phospholipidic bilayer at the beginning (t = 0) and at the end (t = 25 ns) of MDs; F: detail of the polar interactions between **Pro962** and the phospholipidic head or water molecules (red spheres) at the end of the MDs; G: formation of **Ctrl962** aggregates in a chloroform box during 25 ns of MDs (the solvent molecules are omitted for clarity); H: Release profiles of **TK962** from conventional liposome at pH 7.4 (black -◆-) or from **Lipo2-Pro962** incubated at different pHs (red -■- pH = 4; dark blue -●- pH = 5; green -▲- pH = 6.5; gray -x- pH = 7.4). (For interpretation of the references to colour in this figure legend, the reader is referred to the web version of this article.)

also pH-dependent: less than 1% was released within 48 h at pH 6.5, whereas about 50% of **TK962** was released at pH 4.0 and 5.0 . These data suggest that the active compound can be released from the liposomes only after hydrolysis.

To further investigate the effect of the lipophilic anchor, a formulation of liposome loaded with **TK962** (**Lipo1-TK962)** was prepared (see Table S9 for biopharmaceutical features). As reported in Fig. 3H and Table S8, **TK962** was promptly released from **Lipo1-TK962** incubated in physiologic buffer at pH 7.4, as more than 80% of **TK962** was found in the aqueous environment within 48 h.

Interestingly, **Lipo2-Pro962** showed a slower release rate of the drug in comparison with **Lipo1-TK962** (Fig. 3H) even at pH 4.0 and 5.0 at which **Pro962** undergoes very fast hydrolysis when unformulated. Therefore, it can be concluded that the carrier protected, at least

partially, the prodrug from the acid hydrolysis. Therefore, the proposed system was more efficient in preventing fast and premature release of the **TK962** than a classical system where the drug is loaded "as is" in the vesicle. Since **Lipo1-TK962** readily released the loaded drug, no further studies on this formulation were conducted.

3.6. In vitro anticancer activity

TK962, Pro962, **Ctrl962** and their selected liposomal formulations (**Lipo2-Pro962** and **Lipo4-Ctrl962**) were tested *in vitro* using 2D and 3D cell culture models of three different human cancer cell lines. BxPC3 pancreatic adenocarcinoma cell line, k-RAS wild type, was selected because it overexpresses PDGFRβ [43] and was demonstrated to be very sensitive to ours class of TKIs [5]. A431 human squamous cervical

carcinoma cell line, was selected because previous studies showed its sensitivity to our class of TKIs [5]. PSN-1 pancreatic adenocarcinoma cell line was selected because it is similar to BxPC3 but due to k-RAS mutation is more resistant to TKIs.

The dose-response curves reported in Fig. 4 were obtained by 72 h cell incubation with **TK962, Pro962**, **Ctrl962** and their liposomal formulations. Sunitinib (FDA-approved TKI) was used as positive control. The half maximal inhibitory concentration (IC$_{50}$) values calculated by the dose-response curves are reported in Table 2.

Ctrl962 and its liposomal formulation **Lipo4-Ctrl962** were barely cytotoxic against all tested cancer cell lines, either in monolayer or 3D cancer cell model. The lack of significant anticancer activity is consistent with results discussed above showing low kinase target affinity and no drug release by hydrolysis.

Unformulated **TK962** showed cytotoxicity comparable to that previously reported for other members of this class of compounds [5]. A431 and BxPC3 cell lines were comparably sensitive to the TKI, whereas PSN-1 cells were found to be more resistant to the treatment: in the latter cell line, indeed, the highest tested **TK962** concentration reduced the cell viability of about 30% only. These data are comparable to those obtained with Sunitinib (Fig. 4A), suggesting that PSN-1 cells are either less sensitive to the treatment with TKIs or take-up **TK962** lo a lower extent than the other two cell lines. As expected, **TK962** showed only moderate activity in all 3D models, as it reduced the cell viability of about 30–40%, depending on the cell line, at the highest tested concentration. Indeed, it is known that 3D cell models are less sensitive to drug treatment than the monolayer cultures, as the compounds are less able to penetrate the 3D structure [44].

Unformulated **Pro962** exerted a significant cytotoxic effect either in all 2D or 3D cell lines than the parent drug **TK962**, that could be due to enhanced cell internalization of the prodrug driven by the cholesteryl moiety, which may facilitate the anchoring of the prodrug to the cell membrane and the diffusion across 3D systems. Indeed, the CLogP of **Pro962** and **TK962** is 11.79 and 5.25, respectively, and the former has lower aqueous solubility (<1 μM) compared to the latter (65 μM), which

suggest that **Pro962** undergoes higher passive diffusion through the cell membrane than **TK962**, that in turn may result in higher cytotoxic activity. Since **Pro962** was almost equally active against the tested cell lines, the resistance of PSN-1 cells to the treatment with **TK962** can be ascribed to a low uptake of the TKI by this cell line rather than an inefficient inhibition of kinase-mediated pathways.

Lipo2-Pro962 was significantly effective in BxPC3 and A431 bidimensional cell models as compared to unformulated **TK962**, again confirming that reaching an effective internalization of the compound is a main issue with TKI [13]. Notably, **Lipo2-Pro962** displayed high cytotoxicity in the A431 3D system, although inferior to that achieved in the 2D model, suggesting that the lipid vesicles can easily move through this multilayer cellular structure model.

3.7. Association of Lipo2-Pro962 and Lipo4-Ctrl962 with cancer cells

In order to explore the **Lipo2-Pro962** and **Lipo4-Ctrl962** association with cells, flow cytometric studies were carried out by 24 h incubation of **Lipo2-Pro962** and **Lipo4-Ctrl962** fluorescently labelled with rhodamine-DHPE (**Rho-Lipo2-Pro962** and **Rho-Lipo4-Ctrl962)** on A431 cells and PSN-1 cell lines, the most and less sensitive cells among tested lines, respectively. Initially, the effect of serum on **Rho-Lipo2-Pro962** association to A341 cells was investigated by using culture media with normal (RPMI added of 10% FBS) or low (OPTI-mem® added of 1% FBS) serum content (Fig. S7). Indeed, it is well-known that protein adsorption on the surface of nanocarriers may affect their association with cells and in turn their *in vivo* fate [45,46]. Serum protein adsorption on nanoparticles, for example, have been correlated to enhanced internalization of cationic carriers, while opposite effect was observed with anionic nanomaterials [47]. Similar liposome/cell association was found with the two serum compositions (Fig. S7), indicating that the presence of proteins in biological fluids has no effect on the liposome associations with cells. The uptake studies was then repeated in RPMI added of 10% FBS by incubating A431 or PSN-1 cell lines with either **Rho-Lipo4-Ctrl962** or **Rho-Lipo2-Pro962** to evaluate if the

A

B
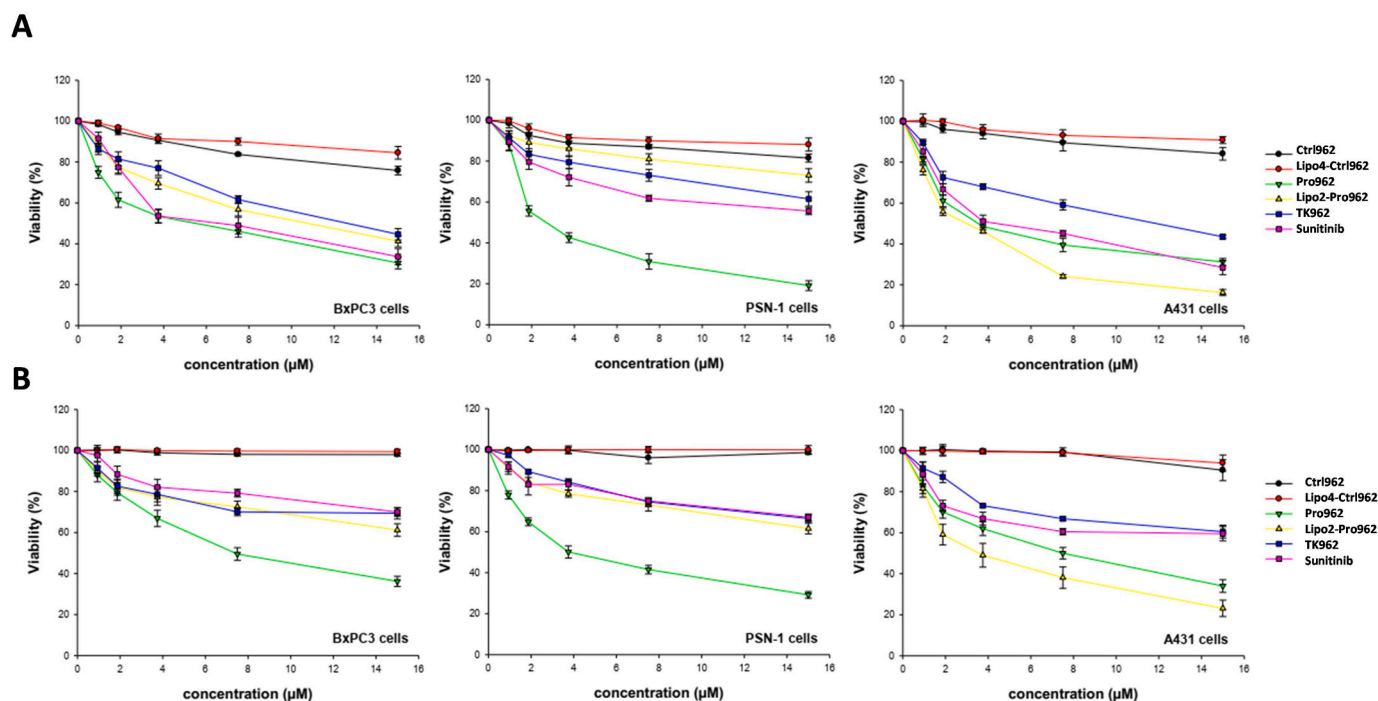
Fig. 4. Cytotoxicity studies in 2D (A) and 3D (B) cell models. A. Cells (3–5 × 10^3 mL^{-1}) were treated for 72 h with increasing concentrations of tested compounds. Cytotoxicity was assessed by 3-(4,5-dimethylthiazol-2-yl)-2,5-diphenyltetrazolium bromide (MTT) test. Error bars indicate the SD. B. Spheroids (2.5 × 10^3 cells/well) were treated for 72 h with increasing concentrations of tested compounds. The growth-inhibitory effect was evaluated by means of the APH test. Error bars indicate the SD.

Table 2

Cytotoxicity of free compounds and selected liposome formulations.

Compound/formulation	IC$_{50}$ μM ± S.D.					
	BxPC3 monolayer	BxPC3 spheroid	PSN-1 monolayer	PSN-1 spheroid	A431 monolayer	A431 spheroid
TK962	11.8 ± 3.2	>15	>15	>15	11.6 ± 2.9	>15
Pro962	4.8 ± 1.3	5.9 ± 1.7	2.7 ± 1.1	3.8 ± 0.8	3.3 ± 0.6	7.5 ± 1.8
Lipo2-Pro962	8.9 ± 1.1	>15	>15	>15	3.1 ± 0.7	3.9 ± 1.1
Ctrl962	>15	>15	>15	>15	>15	>15
Lipo4-Ctrl962	>15	>15	>15	>15	>15	>15
Sunitinib	5.8 ± 1.0	>15	>15	>15	3.9 ± 0.9	>15

lower cytotoxic effect observed with the former formulation (IC$_{50}$ > 15 and 3.3 ± 0.7 for **Rho-Lipo4-Ctrl962** and **Rho-Lipo2-Pro962**, respectively) could be due to a different interaction with cells.

Fig. 5A shows a significant increase of the fluorescence intensity associated to A431 and PSN-1 cells after incubation with **Rho-Lipo4-Ctrl962** and **Rho-Lipo2-Pro962** as compared to control untreated cells, confirming that both formulations efficiently interact with these cell lines. Importantly, a 2-fold higher cell association of **Rho-Lipo2-Pro962** liposomes as compared to **Rho-Lipo4-Ctrl962** was observed in A431 cells, which, in combination with the low potency of **Ctrl962** against isolated kinase, can explain the much higher activity observed with the former formulation. Conversely, in PSN-1 cells, the internalization of **Rho-Lipo2-Pro962** was less effective and comparable to that of **Rho-Lipo4-Ctrl962**. It should be noted that **Pro962** has similar activity in all tested cell lines (see Table 2). On the contrary, the **Lipo2-Pro962** has different activity, which seems to be related to its cellular uptake. Therefore, one can postulate that the lower activity of **Lipo2-Pro962** in PSN-1 cell line is, at least in part, due to a limited uptake in this cell line.

3.8. Metabolic stability

Lipo2-Pro962 formulation and the unformulated **Pro962** and **TK962** were incubated with human plasma for 48 h. No catabolites were found for all the samples. Unformulated **Pro962** was readily hydrolysed to **TK962** (Fig. 6 and Table S10) probably through the action of the hydrolase enzymes present in the plasma while, the **Lipo2-Pro962** remained stable (*i.e.*, no traces of **TK962** were found; Table S8) without **TK962** release for over 48 h.

TK962, **Pro962** and the **Lipo2-Pro962** formulation were exposed to human, rat, or mouse microsomal fractions to evaluate whether the liposomes could protect the TKI scaffold from microsomal enzymes. Microsomal enzymes usually present in the intracellular environment,
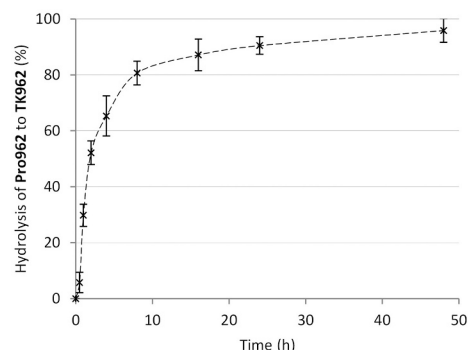
Fig. 6. Hydrolysis of unformulated **Pro962** to **TK962** in human plasma.

being mainly bound to the endoplasmic reticulum membrane, could be involved in degradation of the prodrug released in the lysosomal compartment after liposome uptake. However, Neve et al. [48], reported that different cytochromes can be also associated to the external surface of cells where they are responsible for metabolic transformation of circulating drugs. Accordingly, these experiments were conducted to investigate whether our delivery system could prevent the premature prodrug extracellular oxidative degradation before cell uptake.

After treatment with microsomes, **Pro962** and **Lipo2-Pro962** formulation were acidified to pH 1 to induce the hydrazone bond hydrolysis and consequent release of **TK962** and possibly catabolite(s) thereof from prodrug. This hydrolysis step was performed to unambiguously determine the catabolite(s), if any, derived from biochemical reactions on the kinase inhibitory portion rather than on the lipophilic anchor. HPLC-UV analysis showed that both unformulated **Pro962** and **TK962** undergo time-dependent catabolism (Table S11 and S12),
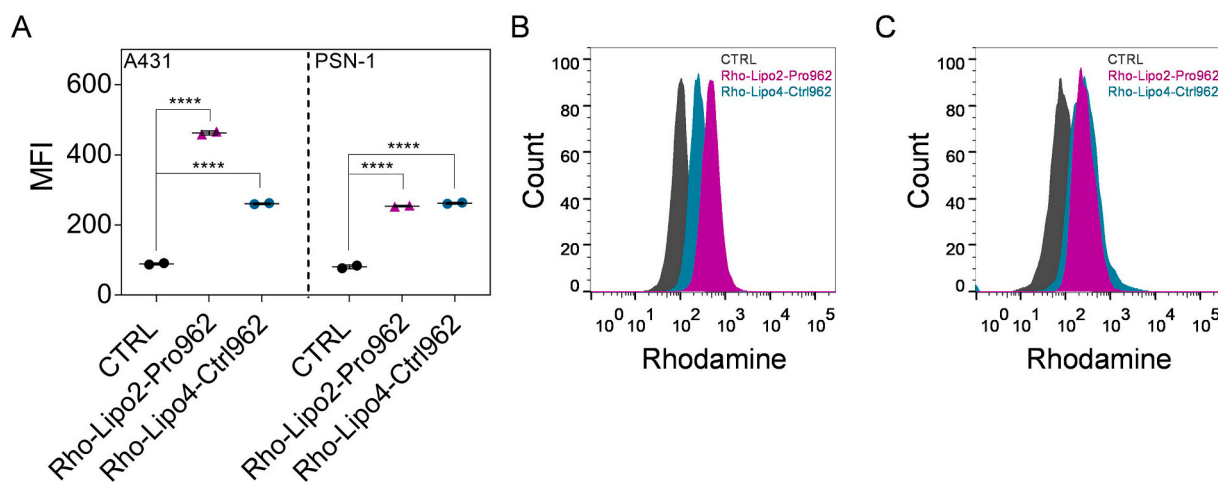
Fig. 5. Quantification *via* Flow cytometry of **Rho-Lipo4-Ctrl962** and **Rho-Lipo2-Pro962** association with A431 and PSN-1 cells after 24 h incubation in RMPI added of 10% FBS. A. Box-and-whisker plots showing a median (centerline) with S.D. of two independent experiments with 3 biological replicates. B-C. Histograms represent flow cytometry results of A431 (B) and PSN-1 (C) cell lines. Cells incubated with culture medium alone were used as control (CTRL). ****$p \leq 0.0001$.

leading to the formation of a more hydrophilic derivative as demonstrated by its shorter elution time in the chromatographic profile with respect to that of **TK962** (Fig. 7A). Conversely, the catabolite could not be detected when **Lipo2-Pro962** was treated with either human or rat microsomes. Treatment with mouse microsomes led to the formation of the same peak observed for **TK962**, although in a lower percentage, which proved that the association of **Pro962** to liposomes offers remarkable protection toward a variety of enzymatic pools contained in microsomes of different species (Fig. 7B) and thus reducing the premature degradation of the prodrug in the extracellular environment.

The effect of human microsomes on **TK962, Pro962** and the **Lipo2-Pro962** formulation were further investigated by means of UHPLC-HRMS/MS analyses, which confirmed the presence of a major catabolite as evidenced by previous HPLC-UV analysis (Fig. 7) and identified the presence of further metabolites for whose molecular structures were proposed.

The analysis of free **TK962** highlighted the generation of at least five different catabolites after the treatment with human microsomes. Fig. 8 shows the different extracted ion chromatograms of the theoretical m/z values (EIC, mass tolerance 10 ppm) corresponding to the identified **TK962** catabolites, simulated by the Biotransformation Mass Defects software to derive their structure. Fig. 8A reports the EIC for m/z 512.1704 at 9.69 min ascribed to the hydrogenation of **TK962** on the ketone function; Fig. 8B reports the EIC at m/z 526.1497 and the two different isobaric chromatographic peaks at 9.76 and 9.98 min assigned to metabolites due to the oxidation occurring in the urea moiety; Fig. 8C reports the EIC at m/z 528.1653 and the two peaks at 8.86 and 8.97 min attributed to the concomitant hydrogenation of the ketone function and the oxidation of the urea moiety, with the consequent formation of two different structural isomers. Details on proposed structures, whose determination was based on MS/MS data acquired in high-resolution mode, are available in Figs. S8–12. Fig. 8D reports the EIC for m/z 510.1548 related to **TK962** and Fig. S13 shows its fragmentation in HR-MS/MS mode. Retention times recorded for all metabolites were lower than that measured for **TK962**, confirming that the formed catabolites were more hydrophilic than **TK962**, as also supported by the proposed structures.

Comparable metabolic profiles were obtained by analysing **Pro962** (m/z 1087.6267 at 13.93 min; Fig. S14E) upon exposure to microsomes and hydrolysis (pH = 1) before injection (Fig. S14) with respect to **TK962**. Indeed, Fig. S14A-D shows the same metabolic pattern, with the

formation of the **TK962** hydrogenated and oxidized catabolites as evidenced by the presence of peaks having the same MS signals and retention times of those previously reported for **TK962**.

While unformulated **Pro962** was found to undergo oxidation even in the absence of microsome enzymes, as indicated by the m/z increase ($\Delta m/z$ of 15.9949 related to the m/z 1103.6216) obtained for the peak at 12.42 min (Fig. S14F), the MS/MS analysis did not provide unambiguous information on the atom involved in the oxidation.

The analysis of **Lipo2-Pro962** treated with human microsomes at different incubation times (0, 10 and 30 min) confirmed that the **Lipo2-Pro962** formulation protected **Pro962** (and, thus, **TK962**) from degradation by microsomal enzymes, as no catabolites were detectable in the samples.

4. Conclusions

The preliminary results reported in this study demonstrated that conventional liposomes loaded with a TKI as **TK962** showed a fast unspecific release of the drug *in vitro*, thus hampering their usefulness as delivery system. However, we also shown that this issue can be circumvented by designing suitable prodrugs. In the case of **TK962,** the use of cholesterol as anchoring moiety to the liposomal bilayer and the use of pH sensitive linker allowed for obtaining a prodrug delivery system (**Lipo2-Pro962**) that was stable in both human plasma and against microsomal enzymes, thus avoiding the uncontrolled release in the blood and the extracellular catabolism of the parent drug. The system was also stable in buffers at pH 7.4 and 6.5, while the drug was efficiently released only in more acidic environment (pH 4.0 and 5.0). Accordingly, the delivery system is supposed to have the potential to specifically release the drugs only in the intracellular environment upon fusion with the lysosomes. Conversely, the slightly acidic tumor environment might cause very limited release of the drug in the extracellular compartment.

Although **Pro962** itself was endowed with promising cytotoxic effect, its instability in human plasma (where the unformulated prodrug was readily hydrolyzed to the parent drug) impairs its further exploitation *in vivo*. Conversely, the liposomal formulation protected **Pro962** from microsome-mediated catabolic degradation and serum enzymes mediated hydrolysis and allowed intracellular delivery to both 2D and 3D cell models of human squamous cervical carcinoma (A431) cells, showing higher cytotoxicity than the parent **TK962**. Overall, our
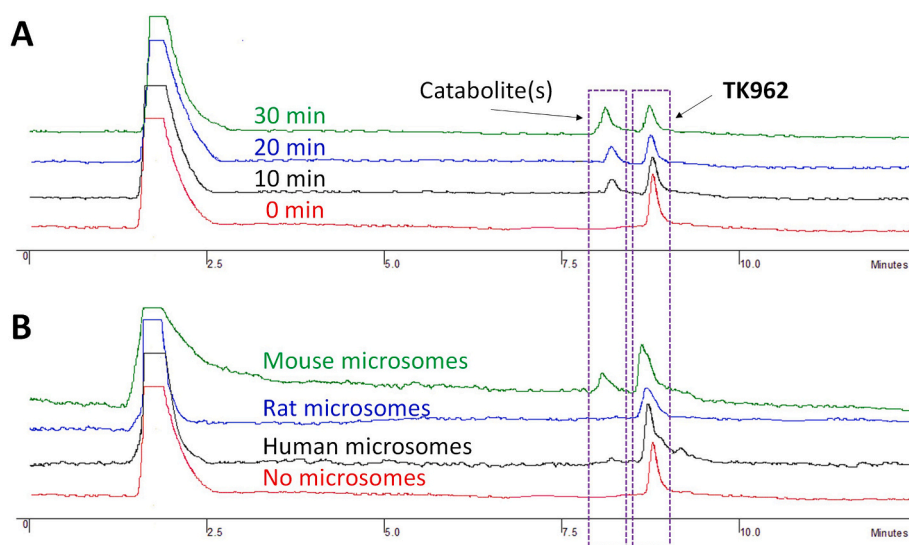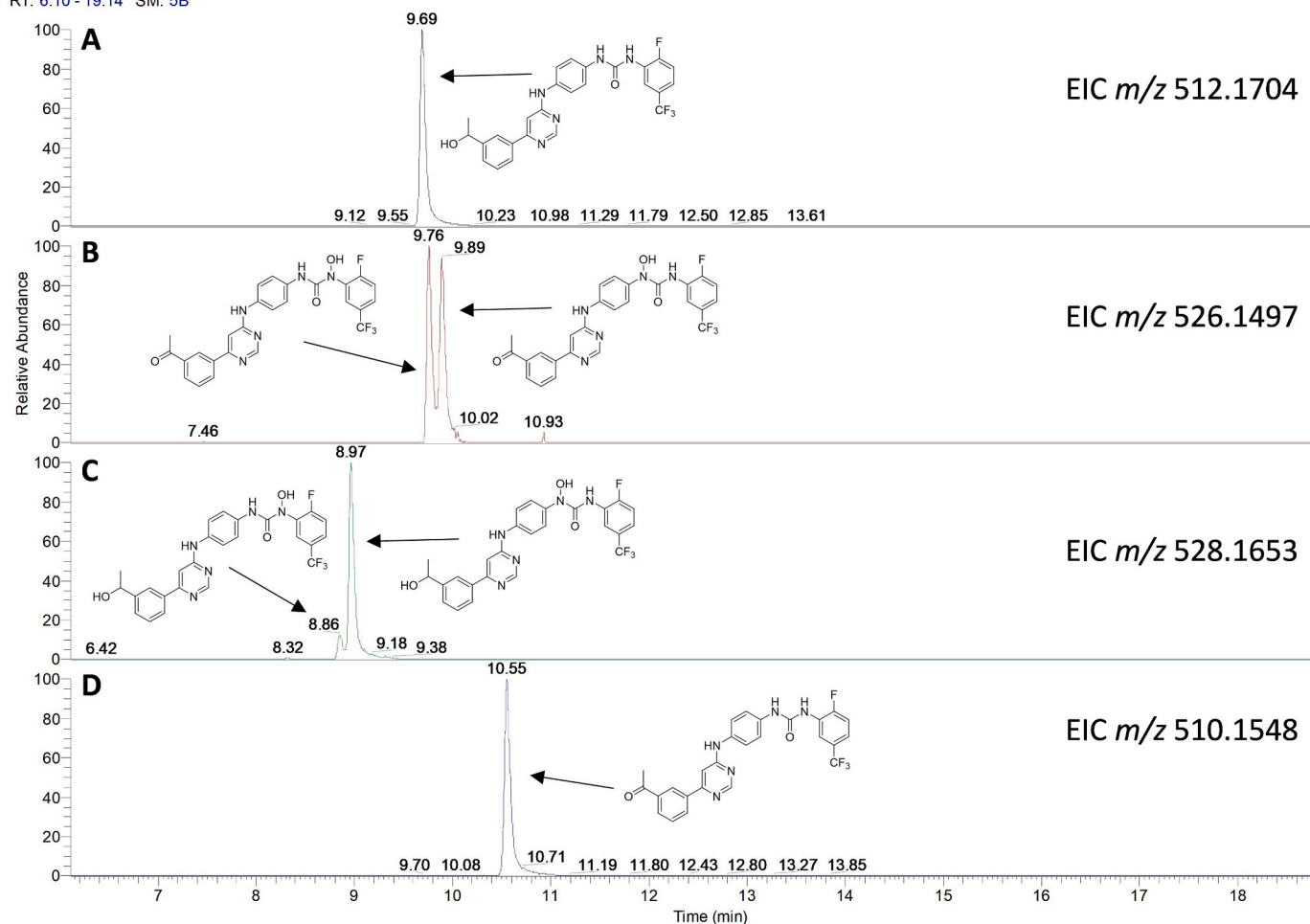

Fig. 7. HPLC-UV chromatographic profile of **TK962** treated with human microsomes (A) and **Lipo2-Pro962** (B) treated with different microsomes for 30 min and subsequent hydrolysis (pH = 1). Treatment of **Pro962** with microsomes at 10, 20 and 30 min and subsequent hydrolysis (pH = 1) led to results comparable to **TK962** (see also Tables S11 and S12).

Fig. 8. Extracted Ion Chromatograms (EIC) after treating **TK962** for 30 min with human liver microsomes. (A) m/z 512.1704 (hydrogenation of **TK962** on the ketone moiety); (B) m/z 526.1497 (oxidation of **TK962** on the urea moiety); (C) m/z 528.1653 (concomitant oxidation and hydrogenation of **TK962**); (D) m/z 510.1548 (**TK962**).

preliminary data suggest that the liposomal formulations of TKIs loaded through hydrolysable lipophilic anchor represents a promising strategy to improve the cellular delivery and the metabolic stability, and thus the efficacy and safety of this class of anticancer drugs. The results obtained with PSN-1 cells suggest that the liposomes by themselves do not guarantee an efficient cellular uptake of the drug as this cell lines did not efficiently incorporate the "raw" carrier, in contrast to what shown by A431 cells. However the development of an effective anticancer therapy was beyond the scope of the work at its present stage, which was to preliminary investigate the usefulness and the importance to prepare suitable TKI prodrugs for the liposome loading. The comparison with conventional liposomes and with unformulated **TK962** and **Pro962** (in particular in terms of protections from unspecific release, enhances stability to oxidative and hydrolytic metabolisms) suggest that the further development of our strategy (*i.e.* conferring stealth properties by PEGylation and introducing targeting agents) for *in vivo* applications is worth addressing. Accordingly, studies on animal models are currently ongoing to further validate this hypothesis.

CRediT authorship contribution statement

Stefano Salmaso: Conceptualization, Methodology, Investigation, Writing – review & editing. **Francesca Mastrotto:** Conceptualization, Methodology, Investigation, Writing – review & editing. **Marco Roverso:** Investigation, Data curation, Writing – review & editing. **Valentina Gandin:** Conceptualization, Investigation, Data curation, Writing – review & editing. **Sara De Martin:** Investigation, Data curation, Writing – review & editing. **Daniela Gabbia:** Investigation, Data curation, Writing – review & editing. **Michele De Franco:** Investigation, Data curation, Writing – review & editing. **Christian Vaccarin:** Investigation, Data curation, Writing – review & editing. **Marco Verona:** Investigation, Data curation, Writing – review & editing. **Adriana Chilin:** Investigation, Data curation, Writing – review & editing. **Paolo Caliceti:** Investigation, Data curation, Writing – review & editing. **Sara Bogialli:** Investigation, Data curation, Writing – review & editing. **Giovanni Marzaro:** Conceptualization, Methodology, Supervision, Resources, Software, Writing – original draft.

Appendix A. Supplementary data

Supplementary data to this article can be found online at https://doi.org/10.1016/j.jconrel.2021.11.006.

References

[1] C. Pottier, M. Fresnais, M. Gilon, G. Jérusalem, R. Longuespée, N.E. Sounni, Tyrosine kinase inhibitors in cancer: breakthrough and challenges of targeted therapy, Cancers (Basel) 12 (3) (2020).

[2] R. Kannaiyan, D. Mahadevan, A comprehensive review of protein kinase inhibitors for cancer therapy, Expert. Rev. Anticancer. Ther. 18 (12) (2018) 1249–1270.

[3] J. Zhang, P.L. Yang, N.S. Gray, Targeting cancer with small molecule kinase inhibitors, Nat. Rev. Cancer 9 (1) (2009) 28–39.

[4] Y. Liu, N.S. Gray, Rational design of inhibitors that bind to inactive kinase conformations, Nat. Chem. Biol. 2 (7) (2006) 358–364.

[5] V. Gandin, A. Ferrarese, M. Dalla Via, C. Marzano, A. Chilin, G. Marzaro, Targeting kinases with anilinopyrimidines: Discovery of N-phenyl-N'-[4-(pyrimidin-4-ylamino)phenyl]urea derivatives as selective inhibitors of class III receptor tyrosine kinase subfamily, Sci. Rep. 5 (2015).

[6] K. Verstraete, S.N. Savvides, Extracellular assembly and activation principles of oncogenic class III receptor tyrosine kinases, Nat. Rev. Cancer 12 (11) (2012) 753–766.

[7] L. Mologni, M. Dalla Via, A. Chilin, M. Palumbo, G. Marzaro, Discovery ofwtRET andV804MRET inhibitors: from hit to Lead, ChemMedChem 12 (16) (2017) 1390–1398.

[8] S. Rudat, A. Pfaus, Y.Y. Cheng, J. Holtmann, J.M. Ellegast, C. Bühler, D. D. Marcantonio, E. Martinez, S. Göllner, C. Wickenhauser, C. Müller-Tidow, C. Lutz, L. Bullinger, M.D. Milsom, S.M. Sykes, S. Fröhling, C. Scholl, RET-mediated autophagy suppression as targetable co-dependence in acute myeloid leukemia, Leukemia 32 (10) (2018) 2189–2202.

[9] I. Plaza-Menacho, L. Mologni, N.Q. McDonald, Mechanisms of RET signaling in cancer: current and future implications for targeted therapy, Cell. Signal. 26 (8) (2014) 1743–1752.

[10] R. Berenstein, Class III receptor tyrosine kinases in acute leukemia - biological functions and modern laboratory analysis, Biomark. Insights 10 (Suppl. 3) (2015) 1–14.

[11] J.T. Hartmann, M. Haap, H.G. Kopp, H.P. Lipp, Tyrosine kinase inhibitors - a review on pharmacology, metabolism and side effects, Curr. Drug Metab. 10 (5) (2009) 470–481.

[12] K.D. Jackson, R. Durandis, M.J. Vergne, Role of cytochrome P450 enzymes in the metabolic activation of tyrosine kinase inhibitors, Int. J. Mol. Sci. 19 (8) (2018).

[13] A.J. Bridges, H. Zhou, D.R. Cody, G.W. Rewcastle, A. McMichael, H.D. Showalter, D.W. Fry, A.J. Kraker, W.A. Denny, Tyrosine kinase inhibitors. 8. An unusually steep structure-activity relationship for analogues of 4-(3-bromoanilino)-6,7-dimethoxyquinazoline (PD 153035), a potent inhibitor of the epidermal growth factor receptor, J. Med. Chem. 39 (1) (1996) 267–276.

[14] J. Blanc Mettral, N. Faller, S. Cruchon, L. Sottas, T. Buclin, L. Schild, E. Choong, A. Nahimana, L.A. Decosterd, Imatinib uptake into cells is not mediated by organic cation transporters OCT1, OCT2, or OCT3, but is influenced by extracellular pH, Drug Metab. Lett. 13 (2) (2019) 102–110.

[15] W.E.A. Ellawatty, Y. Masuo, K.I. Fujita, E. Yamazaki, H. Ishida, H. Arakawa, N. Nakamichi, R. Abdelwahed, Y. Sasaki, Y. Kato, Organic cation transporter 1 is responsible for hepatocellular uptake of the tyrosine kinase inhibitor Pazopanib, Drug Metab. Dispos. 46 (1) (2018) 33–40.

[16] S. Nazir, T. Hussain, A. Ayub, U. Rashid, A.J. MacRobert, Nanomaterials in combating cancer: therapeutic applications and developments, Nanomedicine 10 (1) (2014) 19–34.

[17] C. Zylberberg, S. Matosevic, Pharmaceutical liposomal drug delivery: a review of new delivery systems and a look at the regulatory landscape, Drug Deliv. 23 (9) (2016) 3319–3329.

[18] G. Bozzuto, A. Molinari, Liposomes as nanomedical devices, Int. J. Nanomedicine 10 (2015) 975–999.

[19] J.O. Eloy, M. Claro de Souza, R. Petrilli, J.P. Barcellos, R.J. Lee, J.M. Marchetti, Liposomes as carriers of hydrophilic small molecule drugs: strategies to enhance encapsulation and delivery, Colloids Surf. B: Biointerfaces 123 (2014) 345–363.

[20] M. Alyane, G. Barratt, M. Lahouel, Remote loading of doxorubicin into liposomes by transmembrane pH gradient to reduce toxicity toward H9c2 cells, Saudi Pharm. J. 24 (2) (2016) 165–175.

[21] R.A. Schwendener, H. Schott, Liposome formulations of hydrophobic drugs, Methods Mol. Biol. 605 (2010) 129–138.

[22] R.R. Hood, W.N. Vreeland, D.L. DeVoe, Microfluidic remote loading for rapid single-step liposomal drug preparation, Lab Chip 14 (17) (2014) 3359–3367.

[23] Y. Barenholz, Doxil®–the first FDA-approved nano-drug: lessons learned, J. Control. Release 160 (2) (2012) 117–134.

[24] D.D. Lasic, P.M. Frederik, M.C. Stuart, Y. Barenholz, T.J. McIntosh, Gelation of liposome interior. A novel method for drug encapsulation, FEBS Lett. 312 (2–3) (1992) 255–258.

[25] A.D. Bangham, M.M. Standish, J.C. Watkins, Diffusion of univalent ions across the lamellae of swollen phospholipids, J. Mol. Biol. 13 (1) (1965) 238–252.

[26] K. Dammak, M. Porchia, M. De Franco, M. Zancato, H. Naïli, V. Gandin, C. Marzano, Antiproliferative homoleptic and heteroleptic phosphino silver(I)

complexes: effect of ligand combination on their biological mechanism of action, Molecules 25 (22) (2020).

[27] E. Ramachandran, V. Gandin, R. Bertani, P. Sgarbossa, K. Natarajan, N.S. P. Bhuvanesh, A. Venzo, A. Zoleo, M. Mozzon, A. Dolmella, A. Albinati, C. Castellano, N. Reis Conceição, M.F.C. Guedes da Silva, C. Marzano, Synthesis, characterization and biological activity of novel Cu(II) complexes of 6-Methyl-2-Oxo-1,2-dihydroquinoline-3-carbaldehyde-4n-substituted thiosemicarbazones, Molecules 25 (8) (2020).

[28] M. Floreani, D. Gabbia, M. Barbierato, S.D.E. Martin, P. Palatini, Differential inducing effect of benzo[a]pyrene on gene expression and enzyme activity of cytochromes P450 1A1 and 1A2 in Sprague-Dawley and Wistar rats, Drug Metab. Pharmacokinet 27 (6) (2012) 640–652.

[29] L. Quintieri, M. Fantin, P. Palatini, S. De Martin, A. Rosato, M. Caruso, C. Geroni, M. Floreani, In vitro hepatic conversion of the anticancer agent nemorubicin to its active metabolite PNU-159682 in mice, rats and dogs: a comparison with human liver microsomes, Biochem. Pharmacol. 76 (6) (2008) 784–795.

[30] N.M. O'Boyle, M. Banck, C.A. James, C. Morley, T. Vandermeersch, G. R. Hutchison, Open babel: an open chemical toolbox, J. Cheminform 3 (2011) 33.

[31] O. Trott, A.J. Olson, AutoDock Vina: improving the speed and accuracy of docking with a new scoring function, efficient optimization, and multithreading, J. Comput. Chem. 31 (2) (2010) 455–461.

[32] D. Van Der Spoel, E. Lindahl, B. Hess, G. Groenhof, A.E. Mark, H.J. Berendsen, GROMACS: fast, flexible, and free, J. Comput. Chem. 26 (16) (2005) 1701–1718.

[33] S. Pronk, S. Páll, R. Schulz, P. Larsson, P. Bjelkmar, R. Apostolov, M.R. Shirts, J. C. Smith, P.M. Kasson, D. van der Spoel, B. Hess, E. Lindahl, GROMACS 4.5: a high-throughput and highly parallel open source molecular simulation toolkit, Bioinformatics 29 (7) (2013) 845–854.

[34] S. Sugio, A. Kashima, S. Mochizuki, M. Noda, K. Kobayashi, Crystal structure of human serum albumin at 2.5 A resolution, Protein Eng. 12 (6) (1999) 439–446.

[35] G.M. Morris, R. Huey, W. Lindstrom, M.F. Sanner, R.K. Belew, D.S. Goodsell, A. J. Olson, AutoDock4 and AutoDockTools4: automated docking with selective receptor flexibility, J. Comput. Chem. 30 (16) (2009) 2785–2791.

[36] G. Marzaro, A. Guiotto, M. Borgatti, A. Finotti, R. Gambari, G. Breveglieri, A. Chilin, Psoralen derivatives as inhibitors of NF-κB/DNA interaction: synthesis, molecular modeling, 3D-QSAR, and biological evaluation, J. Med. Chem. 56 (5) (2013) 1830–1842.

[37] K. Vanommeslaeghe, E. Hatcher, C. Acharya, S. Kundu, S. Zhong, J. Shim, E. Darian, O. Guvench, P. Lopes, I. Vorobyov, A.D. Mackerell, CHARMM general force field: a force field for drug-like molecules compatible with the CHARMM all-atom additive biological force fields, J. Comput. Chem. 31 (4) (2010) 671–690.

[38] W. Yu, X. He, K. Vanommeslaeghe, A.D. MacKerell, Extension of the CHARMM general force field to sulfonyl-containing compounds and its utility in biomolecular simulations, J. Comput. Chem. 33 (31) (2012) 2451–2468.

[39] J. Lee, X. Cheng, J.M. Swails, M.S. Yeom, P.K. Eastman, J.A. Lemkul, S. Wei, J. Buckner, J.C. Jeong, Y. Qi, S. Jo, V.S. Pande, D.A. Case, C.L. Brooks, A. D. MacKerell, J.B. Klauda, W. Im, CHARMM-GUI input generator for NAMD, GROMACS, AMBER, OpenMM, and CHARMM/OpenMM simulations using the CHARMM36 additive force field, J. Chem. Theory Comput. 12 (1) (2016) 405–413.

[40] F. Mastrotto, C. Brazzale, F. Bellato, S. De Martin, G. Grange, M. Mahmoudzadeh, A. Magarkar, A. Bunker, S. Salmaso, P. Caliceti, In vitro and in vivo behavior of liposomes decorated with PEGs with different chemical features, Mol. Pharm. 17 (2) (2020) 472–487.

[41] M.W. Karaman, S. Herrgard, D.K. Treiber, P. Gallant, C.E. Atteridge, B.T. Campbell, K.W. Chan, P. Ciceri, M.I. Davis, P.T. Edeen, R. Faraoni, M. Floyd, J.P. Hunt, D. J. Lockhart, Z.V. Milanov, M.J. Morrison, G. Pallares, H.K. Patel, S. Pritchard, L. M. Wodicka, P.P. Zarrinkar, A quantitative analysis of kinase inhibitor selectivity, Nat. Biotechnol. 26 (1) (2008) 127–132.

[42] M.P. Czub, B.S. Venkataramany, K.A. Majorek, K.B. Handing, P.J. Porebski, S. R. Beeram, K. Suh, A.G. Woolfork, D.S. Hage, I.G. Shabalin, W. Minor, Testosterone meets albumin - the molecular mechanism of sex hormone transport by serum albumins, Chem. Sci. 10 (6) (2019) 1607–1618.

[43] H.W. Chung, J. Wen, J.B. Lim, S. Bang, S.W. Park, S.Y. Song, Radiosensitization effect of STI-571 on pancreatic cancer cells in vitro, Int. J. Radiat. Oncol. Biol. Phys. 75 (3) (2009) 862–869.

[44] V. Brancato, J.M. Oliveira, V.M. Correlo, R.L. Reis, S.C. Kundu, Could 3D models of cancer enhance drug screening? Biomaterials 232 (2020) 119744.

[45] M.T. Larsen, M. Kuhlmann, M.L. Hvam, K.A. Howard, Albumin-based drug delivery: harnessing nature to cure disease, Mol. Cell Ther. 4 (2016) 3.

[46] D. Walczyk, F.B. Bombelli, M.P. Monopoli, I. Lynch, K.A. Dawson, What the cell "sees" in bionanoscience, J. Am. Chem. Soc. 132 (16) (2010) 5761–5768.

[47] G. Caracciolo, Liposome-protein corona in a physiological environment: challenges and opportunities for targeted delivery of nanomedicines, Nanomedicine 11 (3) (2015) 543–557.

[48] E.P. Neve, M. Ingelman-Sundberg, Molecular basis for the transport of cytochrome P450 2E1 to the plasma membrane, J. Biol. Chem. 275 (22) (2000) 17130–17135.